A Novel Curvature-Based Algorithm for Automatic Grading of Retinal Blood Vessel Tortuosity

Masoud Aghamohamadian-Sharbaf, Hamid Reza Pourreza, *Senior Member, IEEE*, and Touka Banaee

***Abstract*—Tortuosity of retinal blood vessels is an important symptom of diabetic retinopathy or retinopathy of prematurity. In this paper, we propose an automatic image-based method for measuring single vessel and vessel network tortuosity of these vessels. Simplicity of the algorithm, low-computational burden, and an excellent matching to the clinically perceived tortuosity are the important features of the proposed algorithm. To measure tortuosity, we use curvature which is an indicator of local inflection of a curve. For curvature calculation, template disk method is a common choice and has been utilized in most of the state of the art. However, we show that this method does not possess linearity against curvature and by proposing two modifications, we improve the method. We use the basic and the modified methods to measure tortuosity on a publicly available data bank and two data banks of our own. While interpreting the results, we pursue three goals. First, to show that our algorithm is more efficient to implement than the state of the art. Second, to show that our method possesses an excellent correlation with subjective results (0.94 correlation for vessel tortuosity, 0.95 correlation for vessel network tortuosity in diabetic retinopathy, and 0.7 correlation for vessel network tortuosity in retinopathy of prematurity). Third, to show that the tortuosity perceived by an expert and curvature possess a nonlinear relation.**

***Index Terms*—Curvature, diabetic retinopathy (DR), retinal image, tortuosity measure.**

I. Introduction

DIABETES causes damage in blood vessels. Vessel damages in heart muscles are related to ischemic heart diseases and heart attacks; and vessel damages in the retina cause reduction of sight. The latter called diabetic retinopathy (DR) is one of the common causes of reduction of sight. In fact, many studies show that DR dramatically increases chances of blindness [1] and that it is the leading cause of blindness of the working age especially in developed countries [2]. Presence of numerous microaneurysms is the earliest sign of DR [3]. As the disorder develops, retinal blood vessels become thicker, more twisted and turned [4]. In more advanced levels, neovascularization through inability to provide the required amount of nutrition and oxygen for the retina occurs [5]. These newly generated vessels are very fragile. Therefore, they cause internal bleeding in the retina that endangers the visual system and might ultimately result in blindness.

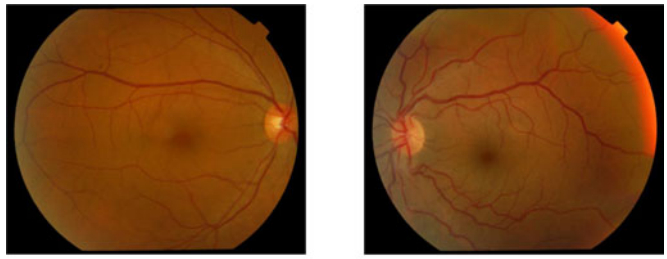

(a) (b)

Fig. 1. Two images of the retina with different tortuosity level. (a) Normal tortuosity. (b) High tortuosity.

Early diagnosis of DR helps controlling its side effects. This is possible with the aid of technical examination of the ocular fundus. Experimentally, it has been shown that when there is no critical symptom of retinal damage, an escalation in retinal blood vessel tortuosity is an early sign of DR [4]. Moreover, presence of tortuous retinal blood vessels is an indicator of retinopathy of prematurity (ROP) in preterm infants [6]. It is well known that in serious cases, ROP causes retinal detachment and blindness [7]. For a detailed review on applications of image processing to diagnosing ROP and comparison of different methods, see [8], [9].

Qualitatively speaking, tortuosity is an indication of how winding a blood vessel is [10]. In Fig. 1, two ocular fundus images with normal and tortuous vessels are shown. As is clear, the vessel network in Fig. 1(b) is more twisted than a normal network that alerts probable presence of DR. Note that vessel tortuosity can happen locally in small portions of blood vessels, or throughout the blood vessel network.

For quantitative measurement of tortuosity, the vessel is modeled as a smooth connected curve. Based on this model, different tortuosity measurement algorithms have been proposed in the literature that could be divided into four general groups:

A. Arc Length Over Chord Length Ratio Methods

Methods of this group have simple mathematical expressions. Lotmar *et al.* [11] were the first to introduce methods of this category and their method was widely utilized thereafter (e.g., [12]–[15]). However, it is apparent that the arc over chord length ratio, on its own, is insufficient for determination of vessels with smooth curvature and vessels with variation in curvature direction. For compensation, Bullit *et al.* [16] and Grisan *et al.* [17] proposed modifications on the approach. In [17], vessels are partitioned into segments with the same convexity and a weighted

Manuscript received October 1, 2014; revised November 30, 2014; accepted January 15, 2015. Date of publication January 23, 2015; date of current version March 3, 2016.

M. Aghamohamdian-Sharbaf and H. R. Pourreza are with the Department of Electrical Engineering, Ferdowsi University of Mashhad, Mashhad 9177948974, Iran (e-mail: masoudas@hotmail.com; hpourreza@ieee.org).

T. Banaee is with the Retina Research Centre, Mashhad University of Medical Sciences, Mashhad 913791-3316, Iran (e-mail: banaeet@mums.ac.ir).

Color versions of one or more of the figures in this paper are available online at http://ieeexplore.ieee.org.

Digital Object Identifier 10.1109/JBHI.2015.2396198

2168-2194 © 2015 IEEE. Personal use is permitted, but republication/redistribution requires IEEE permission.
See http://www.ieee.org/publications_standards/publications/rights/index.html for more information.

sum of arc over chord length of all segments is proposed as a tortuosity measure.

B. Methods Based on Curvature

Curvature is a mathematical measure for how inflected a curve is at a certain coordinate. Hart *et al.* [13] use curvature to propose two tortuosity measures which are the integral of curvature and the integral of curvature squared. For future reference, as in [17], we call these measures τ_c and τ_{sc}. Moreover, the ratio of these integrals over arch or chord length has also been proposed as tortuosity measures in [13]. In [18], the integral of squared curvature derivative is suggested as a measure of tortuosity. These or other curvature-based algorithms have been used in most of the recent works including [19], [20] as well. Curvature-based tortuosity measures are more reliable, but they impose a heavy computational burden compared to the methods of the first group.

C. Methods Based on Angle Variation

These methods compute the direction variations of the vessel to measure tortuosity. In [21], the average of the angles between sample center points that describe the vessel (called local direction variation) was used to measure tortuosity. In [22], the same method is used to measure local angles and the number of times a local angle surpasses $\pi/6$ is considered as tortuosity index.

D. Methods Based on Other Domain

These methods are in fact a subgroup of the curvature-based methods. The difference is that unlike the first group, they calculate curvature in domains beside the space domain. Kaupp *et al.* [23] use Fourier analysis and Ghadiri *et al.* [24] use circular Hough transform to calculate curvature. Moreover, in [25], Non Subsampled Contourlet Transform is used for curvature calculation. The key feature of these methods is evaluation of tortuosity without vessel extraction. However, they suffer from heavy computational burden as well.

There have also been some special cases of tortuosity measurement algorithms. For example, Wallace *et al.* [26] use cubic-spline interpolation for measuring tortuosity. Other work includes [10], [27], [28]. For a more detailed review on different tortuosity measurement algorithms and their applications, see [29].

E. Our Method

Our method is a curvature-based tortuosity measurement; therefore, it falls into the second group. To illustrate the method, in Section II, we define curvature as a mathematical tool for measuring local inflection. To calculate curvature, a novel approach called the template disk method is commonly used. In Section III, after showing the pitfalls of the template disk method, we propose two modifications for amendment of the method. Later in this section, we examine the accuracy of the modified methods using synthetic functions. Section IV deals with how to use the template disk method and its modifications for tortuosity measurement, and finally in Sections V and VI, the test results, the concluding remarks, and possible future works are given.

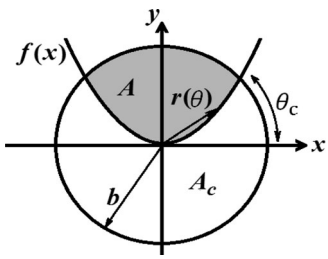

Fig. 2. Curvature calculation with the template disk method.

II. Curvature Calculation

Curvature is an indication of local twistedness of a curve [30]. In the continuous case, for a planar curve $y = f(x)$, curvature is given by

$$\kappa = \frac{y''}{(1+y'^2)^{3/2}}. \tag{1}$$

Moreover, for the parametric representation $x = x(t)$ and $y = y(t)$, we have

$$\kappa = \frac{y''(t)x'(t) - x''(t)y'(t)}{(x'(t)^2 + y'(t)^2)^{3/2}}. \tag{2}$$

Note that rigid transformations would not affect the absolute value of curvature. However, the sign may change by rotation.

To calculate curvature using a discrete model of a curve, numerical approaches have been exploited in [31]. However, numerical methods are nontrivial and time consuming for large datasets [32]. An elegant method for estimation of curvature that has a relatively low computational complexity was introduced in [33]. This approach, known as the template disk method, is further explored for 2-D images in [34]. Through its simplicity, this method has been widely utilized in most applications requiring curvature calculation. The basic idea of the method is to relate the area between the curve and a template disk of a suitable radius with curvature. To illustrate the method, note that for a point with zero first derivative, we have

$$\kappa = f''(x). \tag{3}$$

Hence, to calculate curvature for a point (x, y), first a template disk of radius b is sketched around the point (see Fig. 2). Next, the center of the Cartesian coordinate system is set on the point to ensure that $f(0) = f'(0) = 0$. Under this assumption, Taylor series for points in the vicinity of zero is

$$f(x) = 0 + 0 + \frac{1}{2}\kappa x^2 + o(x^3) \tag{4}$$

where κ denotes curvature at the origin and $o(x^3)$ expresses higher order terms of the series. Using polar coordinates (r, θ), we have

$$r\sin\theta = \frac{1}{2}\kappa r^2\cos^2\theta + o(r^3\cos^3\theta). \tag{5}$$

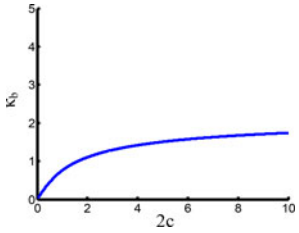

Fig. 3. Estimated curvature versus analytical curvature for a parabola.

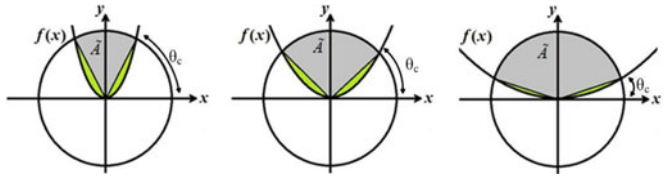

Fig. 4. Approximating area A using the crossover point of the curve and the template disk.

Normalizing the coordinate system by the radius of the template disk b, we get

$$R\sin\theta = \frac{1}{2}KR^2\cos^2\theta + o(R^3\cos^3\theta) \tag{6}$$

where $R = r/b$ and $K = \kappa b$. Now, assume that θ is near zero, we can approximate $\cos\theta$ by one and $\sin\theta$ by θ and define θ as a function of *R* and *K*

$$\theta(R) \approx \sin^{-1}\left[\frac{1}{2}KR + o(R^2)\right]. \tag{7}$$

Using this expression, we could approximate area *A*, which is the area between the disk and the curve. Define:

$$a = \int_0^1 RdR \int_{\theta(R)}^{\pi-\theta(R)} d\theta \tag{8}$$

then $A = ab^2$. As it turns out, analytical calculation of this integral does not yield a linear relation between curvature and this area. However, if $\theta(R)$ is further approximated by its Taylor series around zero, we get

$$\theta(R) \approx \frac{1}{2}KR + o(R^2). \tag{9}$$

Ignoring higher order terms, the normalized area using (8) is

$$a \approx \frac{\pi}{2} - \frac{K}{3} \tag{10}$$

and rearranging terms yield

$$\kappa \approx \frac{3\pi}{2b} - \frac{3A}{b^3} = \frac{3A_c}{b^3} - \frac{3\pi}{2b} \tag{11}$$

where A_c is the complement of A. Therefore, $\kappa \propto A_c$. Based on this relation and the argument given in the next section, the nonlinear estimation of curvature κ_{nl} is defined as

$$\kappa_{nl} \triangleq A_c. \tag{12}$$

III. Modifications of the Template Disk Method

As we saw in the previous section, the assumption that θ is small simplifies (6) and results in (7). However, this assumption is valid merely if curvature is sufficiently small. To show that (11) fails to deliver for large curvature, assume that κ_{nl} is used to estimate the curvature of a parabola $y = cx^2$ at the origin. Fig. 3 is a comparison of the analytical curvature *2c* (horizontal axis) versus curvature derived by the method. As is clear, though for small curvature (small c) estimated curvature and actual curvature are proportional, the relation for large curvature is far from being linear. On the other hand, as indicated by the test results of [34], for error free calculation of curvature in digital images, the radius of the template disk should be large. This is due to the fact that for small radius, area calculation may contain significant error. However, as b increases, area *A* has weaker dependency on κ. Therefore, we face a contradiction between the assumption that simplifies (7) (which assumes a small radius for the disk) and the one that is required for accurate implementation (which requires a large radius for the template disk).

Although we showed that the template disk method is inaccurate when estimation of high curvature is concerned, through its simplicity, we try to perform the necessary modifications in order to make it applicable to all curvature values. In what follows, two modifications are given.

A. First Modification: Based on Crossover Point (κ_{cp})

As Fig. 4 shows, irrespective of θ_c (the crossover angle of the curve and the disk), the area between the curve and the template disk is the gray area plus the green area. Therefore, area A could be approximated by the gray area or $\tilde{A}$. In what follows, we try to relate $\tilde{A}$ and θ_c.

To derive θ_c, it suffices to set $R = 1$ in (6). We have

$$\sin\theta_c = \frac{1}{2}K\cos^2\theta_c + o(\cos^3\theta_c). \tag{13}$$

Now, we assess three different cases:

1) θ_c Near Zero: In this case, $\sin\theta_c$ is approximated by θ_c and $\cos\theta_c$ by one. We have

$$\theta_c = \frac{1}{2}K. \tag{14}$$

Thus, $\tilde{A}$ is

$$\tilde{A} \approx \frac{\pi b^2}{2} - \frac{Kb^2}{2}. \tag{15}$$

Rearranging terms yields the following relation for small crossover angle:

$$\kappa \approx \frac{\pi}{b} - \frac{2\tilde{A}}{b^3}. \tag{16}$$

Note that as was expected, this equation is similar to (11) neglecting a scaling factor.

2) θ_c Near $\pi/2$: If θ_c is near $\pi/2$, we can approximate $\cos\theta_c$ by $\frac{\pi}{2} - \theta_c$ and $\sin\theta_c$ by one that yields

$$\theta_c \approx \frac{\pi}{2} - \sqrt{\frac{2}{K}}. \tag{17}$$

Hence, curvature for such angles has the following relation with $\tilde{A}$:

$$\kappa \approx \frac{2b^3}{\tilde{A}^2}. \tag{18}$$

As (16) and (18) indicate, for small curvature (i.e. small crossover angle), κ has a linear relation with A (or $\tilde{A}$). However, for large curvature (i.e., large crossover angle), κ is proportional to the squared reciprocal of A (or $\tilde{A}$). We define the squared reciprocal of A as an approximation of curvature

$$\kappa_{cp} \triangleq \frac{1}{A^2}. \tag{19}$$

Note that for small curvature, A is relatively large that results in a κ_{cp} close to zero. Therefore, (19) should have satisfactory accuracy for small curvature as well. For this reason, we consider (19) it as a suitable alternative for (12). The test results of Section III-C will manifest that this presumption is in fact valid.

3) Other Values of θ_c: As we will show with sufficient tests, the metric κ_{cp} has sufficient accuracy for values which are neither close to 0 nor close to $\pi/2$. Therefore, no further expression is required to treat such other angles.

B. Second Modification: Trigonometrical Method (κ_{tr})

Returning to (13), if we neglect $o(R^3\cos^3\theta_c)$, we have the following relation between θ_c and K:

$$K \approx \frac{2\sin\theta_c}{\cos^2\theta_c} \Longrightarrow \kappa \approx \frac{2\sin\theta_c}{b\cos^2\theta_c}. \tag{20}$$

Using (20), we can directly relate curvature to the crossover angle. Hence, define

$$\kappa_{tr} \triangleq \frac{2\sin\theta_c}{1-\sin^2\theta_c}. \tag{21}$$

To compare the three curvature estimation methods, note that the first two methods rely on area calculation which is a form of integration. Therefore, we expect these two methods to be resilient against noise and return smoother results. On the other hand, to get accurate results using the third method, knowledge of the exact crossover point is a fundamental requirement. Therefore, even quantization error may widely affect the results. This phenomenon will be explored in the next section. However, this method does not need area calculation which is an advantage in terms of implementation. Based on the aforesaid facts, if we should deal with noise-free signals of relatively low curvature, κ_{tr} should produce better results. However, for signals sampled in the presence of noise, κ_{cp} should function better.

C. Accuracy Examination Using Synthetic Functions

In this section, we compare the two modified template disk methods with the basic method. To do so, we use synthetic parabolas, circles and sinusoids. Note that even though for each method the resultant range of values may be different, in our analysis of tortuosity linear proportionality to real curvature is of mere importance. Hence, all test results to be presented are suitably normalized.

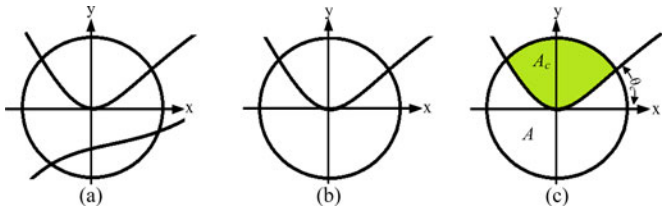

Fig. 5. Curvature estimation with the template disk method (a) Drawing the template disk. (b) Eliminating the inferior segment from inside the disk. (c) Determining A, A_c, and θ_c.

In order to estimate curvature for a point on the curve $y = f(x)$, first a circle with center (x, y) and radius b is depicted on the curve [see Fig. 5(a)]. Next, the segment of the curve inside the disk that is connected to the point (x, y) is saved and the rest of the curve is eliminated [see Fig. 5(b)]. At this point, the two areas confined within the disk and the curve are calculated. The larger area is A_c and the smaller one is A. Moreover, the crossover point of the curve and the disk is used to derive θ_c and this angle is used for calculation of κ_{tr}.

1) Parabola: For a parabola $y = cx^2$ with $c > 0$, curvature for $x = 0$ using (1) is

$$\kappa = 2c. \tag{22}$$

Fig. 6 shows the estimated curvature versus analytical curvature for $0.001 \leqslant c \leqslant 1.5$ for four different template disk radii. As can be seen (and this was shown beforehand) curvature and κ_{nl} are not proportional. On the other hand, κ_{cp} and κ_{tr} elevate linearly with analytical curvature. In fact, for small curvature, all three methods show proportionality to real curvature. However, as curvature increases, only the two modified methods maintain their linearity. Note that the stepwise behavior of κ_{tr} is due to the quantization of values of θ_c. For larger values of c, even small changes in θ_c highly affect the denominator of (21). Therefore, the quantization error for such values is significant.

2) Circle: To estimate curvature for a circle, assume the following equation for a circle that is tangent to the origin:

$$(y-r)^2 + x^2 = r^2 \qquad r \gg b \tag{23}$$

where r is the radius of the circle. Using (1), curvature at the origin is

$$\kappa = 1/r. \tag{24}$$

Fig. 7 shows the estimated curvature versus analytic curvature for $20 \leqslant r \leqslant 200$ for three different values of b. Relatively low values of curvature for a circle imply that all three methods should return acceptable results. Note that κ_{tr} is still suffering from quantization error.

3) Sinusoid: One of the functions that is commonly used for examination of the accuracy of a tortuosity measure is a sinusoid. If a sinusoid is given by $y = A_m\sin(\omega x)$, then curvature for every point using (2) is

$$|\kappa| = \left| \frac{A_m\omega^2\sin(\omega x)}{(1 + A_m^2\omega^2\cos^2(\omega x))^{3/2}} \right|. \tag{25}$$

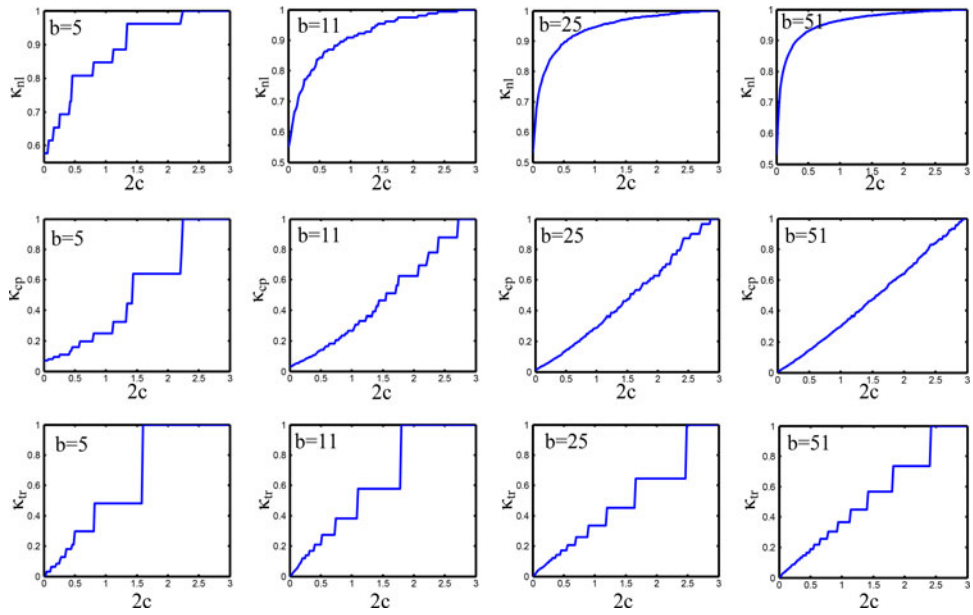

Fig. 6. Estimated curvature with κ_{nl}, κ_{cp}, and κ_{tr} versus actual curvature for a parabola.

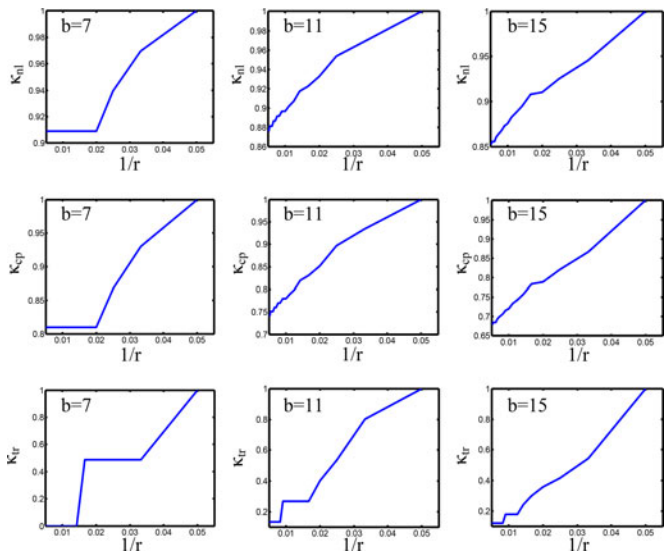

Fig. 7. Estimated curvature with κ_{nl}, κ_{cp}, and κ_{tr} versus actual curvature for a circle.

With three tests, we compare the analytical curvature with κ_{nl}, κ_{cp}, and κ_{tr}. In the first test, we compare (25) with the outcome of the three methods for a specified frequency and amplitude. In the next two tests, we employ an image of a sinusoid and observe the effect of amplitude and frequency variation on the estimated curvature. To do so, the average value of curvature for each image is calculated. Note that as Grisan *et al.* [17] claim, increase in amplitude or frequency should increase average curvature. Detailed description of each test is given below.

4) First Test: Fig. 8 shows the graph of $|\kappa|$ and results of point-wise curvature calculation with each method for a sinusoid with $A_m = 200$ and $\omega = 2\pi/100$, where b is 11 pixels. It is clear that κ_{cp} is most similar to real curvature and curves of κ_{tr} and κ_{nl} are very much alike.

5) Second Test: For this test, first a 500×500 pixel image containing a sinusoidal curve is created. Next, the period of the sinusoid is held fixed at 100 pixels and its amplitude is varied from 50 to 200 pixels. For each method, mean curvature of each image using a template disk of radius 11 is depicted in Fig. 9. As the figure shows, elevation in average curvature with amplitude increment is more apparent for κ_{tr} than κ_{cp} and κ_{nl}.

6) Third Test: For this test, the same image as the second test was used. Only this time, the amplitude is fixed at 100 pixels and the period is changed from 50 to 250 pixels. Using a template disk of radius 11, mean curvature of each image was calculated (see Fig. 10). As can be seen, proportionality between frequency and curvature is better seen for κ_{tr} and κ_{cp}.

IV. Tortuosity Evaluation

In this section, we propose an algorithm for automatic evaluation of tortuosity in retinal images. Since curvature calculation is the core of this algorithm, all three curvature estimation methods given in Section III are used so as to test their performance in the algorithm. The algorithm contains the following steps:

1) Vessel detection.
2) Extraction of vascular skeleton.
3) Elimination of crossovers and bifurcations.
4) Local and global tortuosity measurement.

A. Vessel Detection

For vessel detection, we use the algorithm in [35]. To detect a vessel map using this algorithm, first the green layer of the RGB representation of the image is extracted. The significant property of this plane is that the vessel and the background possess the highest contrast. Next, this plane is divided into a number of overlapping blocks and by placing a circular mask, the Radon transform for each block is calculated. The angle for which the local sinogram reaches its maximum value is the

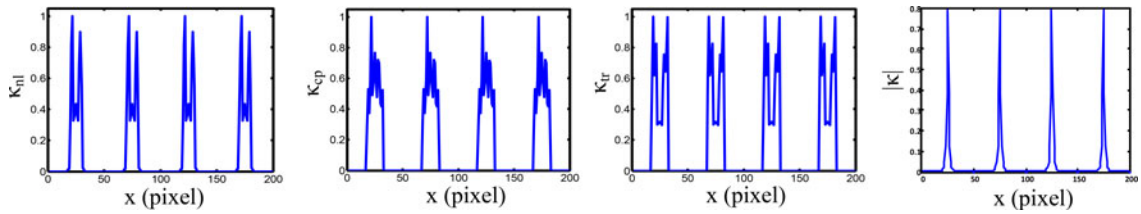

Fig. 8. Point-wise estimated and analytical curvature for a sinusoid ($b = 11$, $A_m = 200$, and $\omega = 2\pi/100$).

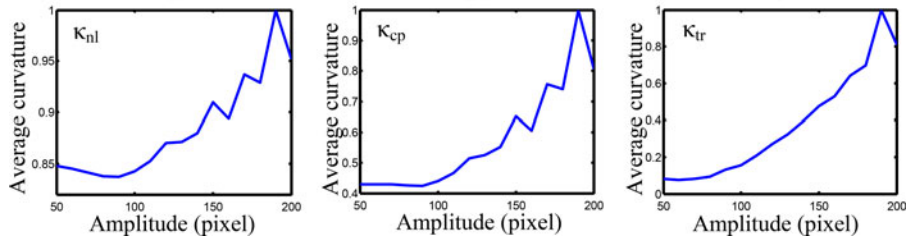

Fig. 9. Effect of amplitude increment on estimated average curvature for a sinusoid ($b = 11$ and $\omega = 2\pi/100$) .

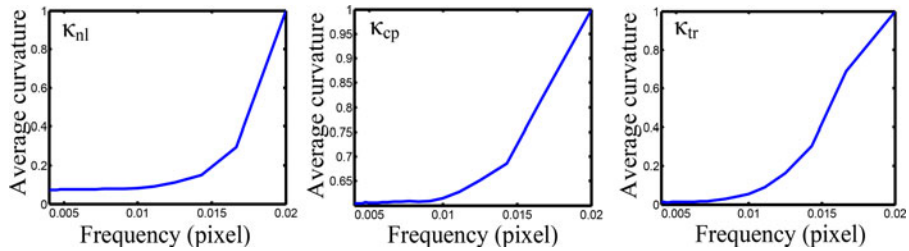

Fig. 10. Effect of frequency increment on estimated average curvature for a sinusoid ($b = 11$ and $A_m = 100$).

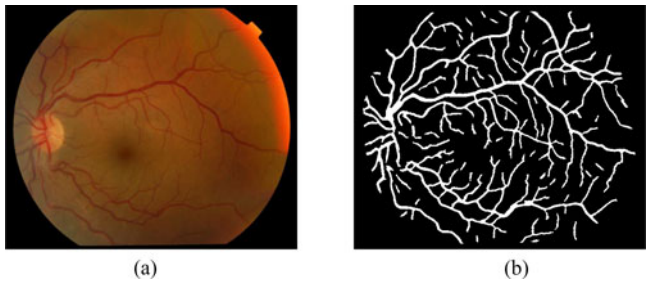

Fig. 11. Vessel detection algorithm. (a) Retinal Image. (b) Vessel map.

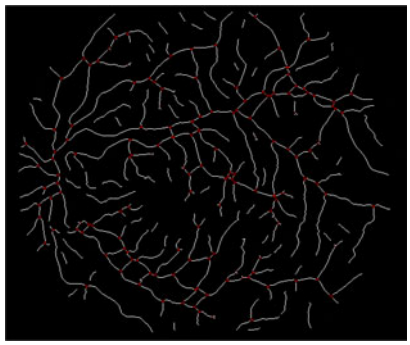

Fig. 12. Bifurcation and crossover detection for the vessel map of Fig. 11.

direction perpendicular to a vessel. By verifying the presence of a vessel, a linear approximation of the vessel is depicted and Combination of these local linear vessels gives the vessel network. Fig. 11 shows an image of a retina and the resultant vessel map. Smoothing effect of Radon transform is the reason why this method is so powerful in presence of noise.

B. Extraction of Vascular Skeleton

In order to use the curvature calculation methods described in Section III, it is necessary to thin the vessel map and extract the vessel skeleton. For this end, morphologic thinning algorithm suggested in [36] is used.

C. Elimination of Crossovers and Bifurcations

Bifurcation and crossover of the vessels could trouble the tortuosity evaluation process. Therefore, prior to curvature estimation procedure, all areas containing bifurcation and crossover should be eradicated. To detect such areas, a circle is drawn at every point on the map and the number of crossovers of the disk and the map is counted. If this number is three or four, bifurcation and/or crossovers in that area is detected. Fig. 12 shows the outcome of implementing the algorithm for the vessel map of Fig. 11.

TABLE I
BEST SRCC REPORTED BY [17] AND [37] FOR THE RET-TORT DATASET AND SRCC FOR OUR ALGORITHM

Tortuosity Measure	Arteries	Veins
Grisan	0.949	0.853
Quadratic polynomial decomposition [37]	0.944	0.828
τ_c over chord length	0.939	0.842
τ_{sc} over chord length	0.928	0.804
τ_{sc}	0.925	0.826
τ_c	0.922	0.837
Average angles [21]	0.920	0.814
τ_{nl}	0.945	0.840
τ_{cp}	0.928	0.830
τ_{tr}	0.924	0.851

D. Local and Global Tortuosity Measurement

To calculate global tortuosity of a vessel map, first local tortuosity for each point on the map is calculated using κ_{nl}, κ_{cp}, and κ_{tr}. Here, we propose the following formula for measuring global tortuosity:

$$\tau = \frac{1}{m}\sum_{i=1}^{m}\kappa_i \tag{26}$$

where κ_i denotes curvature for the ith point on the map and m denotes the total number of points for which curvature is measured. Based on the three methods of local tortuosity calculation, global tortuosity measures are called τ_{nl}, τ_{cp}, and τ_{tr}.

V. RESULTS AND CONCLUSION

In this section, we compare the performance of our algorithm with the state of the art. Comparison is made both on the vessel level and on the vessel network level. We show that our algorithm matches the best of the state of the art when tortuosity of single vessels is considered. Further, we compare our method with subjective results for the vessel network case. To assess correlation with subjective results, we use Spearman's rank correlation coefficient (SRCC), which is an indicator of the linear relation between two datasets. Further, we report the probability of null hypothesis (or $p-$value) for each case to ensure that there is no stronger nonlinear relation between any two compared datasets. Note that if this number is below 0.05, it is guaranteed that no such nonlinear relation exists.

A. Vessel Level Tortuosity

To evaluate the vessel level performance of our algorithm, we conducted it on the RET-TORT data bank. This data bank is the image bank introduced by Grisan *et al.* [17] and contains 30 images of arteries and 30 images of veins, sorted based on the tortuosity level of the images.

Table I shows SRCC for our algorithm and some of other state of the art. It is apparent that τ_{nl} closely accommodates with the expert's opinion for the artery images. Further, τ_{tr} has the best correlation for the vein images while τ_{nl} is a reliable choice as well. Therefore, when tortuosity of single vessels is concerned, Grisan's algorithm and τ_{nl} are as good in terms of correlation. Note that the results suggest a strong nonlinear relation between perceived tortuosity of the arteries and curvature. However, the relation for the veins is uncertain (both linear and nonlinear metrics are comparable).

B. Vessel Network Tortuosity

An important purpose of introducing a tortuosity measurement algorithm is to calculate the entire vessel network tortuosity of the retina. Since on the vessel level test, Grisan's algorithm has the best performance, it is the best candidate for extension to the vessel network case. To extend Grisan's algorithm to the entire vessel network, the following issues should be considered:

1) Since the algorithm is vessel based, identification and separation of all vessels is most likely a requirement for vessel network implementation. This is a tough and time consuming task (see [38]).
2) In [17], Grisan has not specified how their algorithm deals with vessel bifurcation and/or crossover. Specifically, for vessel bifurcation, the assignment of tortuosity is not clear.
3) Grisan's algorithm requires segmentation of a vessel based on convexity change. Further, arc and chord length calculation of each segment is a requirement for measuring the tortuosity of each vessel. Therefore, the algorithm requires two additional steps compared to ours to reach the same level of correlation.

These are our objections to [17] when extension to the vessel network case is considered. Finally, since [17], Grisan has only manually segmented a vessel map to measure whole image tortuosity (e.g., [39]) and has not yet introduced a fully automatic method (to our knowledge) for this task. Therefore, a quantitative comparison of our algorithm with Grisan's is impossible unless they extend their method to the vessel network case.

To evaluate the performance of our algorithm when measuring vessel network tortuosity in DR, we used a data bank that contains ten full images of the retina with a 2050×1748 pixel resolution. This dataset is produced in Khatam-Al-Anbia hospital of Mashhad and is sorted based on tortuosity by a number of experienced experts with focus on the subject of DR. We have provided this dataset and the votes of the experts at www.eiarg.um.ac.ir. In order to decrease the computational burden, we lowered the resolutions to 575×479. We should also mention that the SRCC between the votes of the experts for this dataset ranges from 0.758 to 0.964 (p-value < 0.01), which suggests a fairly good agreement among experts.

Table II is a comparison of SRCC for the three metrics. As the numbers indicate, τ_{nl} is strongly correlated with the experts' opinion especially when the average vote is considered. This excellent correlation manifests the power of our algorithm in grading the tortuosity of retinal blood vessel networks. The interesting point is that in this test, the nonlinear method is more capable of following the opinion of each expert rather than the linear methods. Hence, we conclude that the opinion of an expert possesses a nonlinear relation with curvature (or a linear relation with area A). In fact, when estimated curvature maintains a linear relation with real curvature, results are of weaker correlation.

TABLE II
SRCC OF THE ESTIMATED VESSEL NETWORK TORTUOSITY WITH SUBJECTIVE RESULTS FOR THE SECOND DATASET ($p-$VALUES$< 6 \times 10^{-3}$)

	τ_{nl}	τ_{cp}	τ_{tr}
Exp. 1	0.939	0.927	0.915
Exp. 2	0.939	0.891	0.878
Exp. 3	0.903	0.903	0.854
Exp. 4	0.891	0.7939	0.8788
Exp. 5	0.818	0.830	0.866
Overall vote	0.946	0.915	0.925

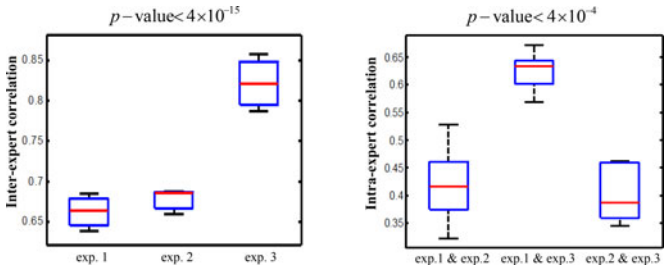

Fig. 13. Boxplot of (a) interexpert correlation and (b) intraexpert correlation.

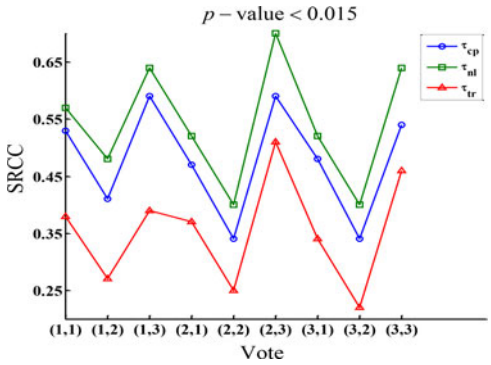

Fig. 14. SRCC of each vote the experts with subjective results for the third dataset (Note that the pair (i, j) on the horizontal axis denotes the ith vote of the jth expert).

TABLE III
SRCC OF EACH METHOD WITH AVERAGE VOTE OF THE EXPERTS FOR THE THIRD DATASET ($p-$VALUES< 0.002)

	τ_{nl}	τ_{cp}	τ_{tr}
Exp. 1	0.61	0.56	0.41
Exp. 2	0.48	0.41	0.28
Exp. 3	0.7	0.61	0.48
Overall average vote	0.71	0.61	0.47

To evaluate the performance of our algorithm in measuring the tortuosity of ROP images, we conducted it on a third data bank that contains 120 full images of the retina. The goal of the test is to determine the positive cases of ROP among the images. All images of this dataset belong to preterm infants and we have provided the dataset at www.eiarg.um.ac.ir. We asked three ophthalmologists on three different occasions to give us their opinion on existence of tortuosity by assigning one and zero to the positive and the negative cases, respectively. Further, we used the three methods to measure tortuosity for the entire vessel network.

A full statistical analysis of the votes is given in Fig. 13. As is clear from the figure, interexpert correlation is not high enough to ensure sufficient consistency for each individual expert. Further, when correlation with other experts is considered, a dramatic decline is observed. Therefore, we conclude that when it comes to diagnosing the tortuosity of ROP, the problem (as stated in [40] as well) is the absence of agreement among experts rather than the metric itself. Irrespective of the above discussion, as Fig. 14 indicates, τ_{nl} is most capable of following each vote of all experts. However, correlation is significant for experts 1 and 3, and is relatively weak for expert 2. Moreover, if we consider 0.5 as a threshold for good correlation, it is easy to see that while correlation between the experts is mostly weak (see Fig. 13), τ_{nl} is (to a great extent) capable of keeping itself correlated with each individual expert at all occasions (see Fig. 14). From another point of view, when the average vote of each expert is considered, as Table III indicates, τ_{nl} is superior to the other two methods and its correlation ranges from good to strong. Finally, for the average vote of all experts, SRCC for τ_{nl} is 0.701, which (considering the inconsistency of the votes) suggests a strong correlation between the average vote and this metric. This strong correlation manifests the capability of our algorithm in determining the positive cases of tortuosity in ROP images. Moreover, based on the results we have from all three tests, we conclude that tortuosity and curvature possess a nonlinear relation.

To compare the computation time of the given three algorithms, the total performance time of the algorithms on the ten images of the second data bank was measured. The program was written as single thread in MATLAB R2012 and was ran on a computer with Corei5-3570K CPU. The running time for all measures were approximately the same and was nearly 35 s (3.5 s /image). We should mention that a MATLAB implementation of our algorithm is available at www.eiarg.um.ac.ir. We encourage the research society to use our algorithms and publish their results. Further, we encourage using the two introduced datasets for comparison tests in the future.

In this paper, we presented a fully automatic algorithm for evaluating tortuosity in retinal images. Our algorithm is a curvature-based algorithm. For curvature calculation, we used the template disk method. We presented two modifications on this method to correct the nonlinearity of template disk method against curvature and assessed the linearity of results with numerous tests. Finally, we used all three methods for measuring tortuosity of retinal images. In doing so, we showed that tortuosity has a nonlinear relation with curvature. No requirement for classification of vessels as opposed to vessel based measures, simplicity of the measure, low-computational burden, and an excellent matching to the clinically perceived tortuosity of the retinal blood vessels are the major features of the algorithm proposed in this paper.

VI. Future Works

We believe the following issues need more in-depth analysis and consideration:

1) Relation Between Tortuosity of Arteries and Vessel Network Tortuosity: Note that both vessel network tortuosity and tortuosity of arteries are highly correlated with a nonlinear function of curvature. Therefore, it seems that the state of arteries have a major impact on vessel network tortuosity. This is due to the observation that even though τ_{nl} does not follow the tortuosity of veins as well as the arteries, the vessel network tortuosity is still very well followed by this metric.

2) Relation Between Nonlinear Curvature and Caliber of Vessels: As Trucco *et al.* [10] claim, while measuring the tortuosity of a vessel network, more attention should be given to the thicker vessels, which is possible by introducing a weighting system. It seems that τ_{nl} provides such a weighting as wll. This is due to the observation that usually thinner vessels are more tortuous than thicker vessels and the fact that κ_{nl} saturates for high curvature suggest a reduction of curvature for such vessels (same as assigning a smaller weight to these vessels). Therefore, the nonlinear method provides a natural filtering to ensure that the assigned tortuosity to a vessel is related to the caliber of that vessels. By proving this, we will be able to explain the reason why tortuosity and curvature possess a nonlinear relation.

3) Fitting a Model to Veins and Arteries: Based on the results for synthetic functions (see Section III-C), it seems that the best mathematical model for a vein is a sinusoidal. For the arteries, however, a parabola might be a better choice since τ_{nl} has the best correlation with subjective results.

Acknowledgment

The authors would like to thank M. Abrishami and H. Hosseini (Retina Research Centre, Mashhad University of Medical Sciences, Mashhad, Iran), M. K. Mathews (University of Maryland, College Park, MD, USA), S. Russell (University of Iowa, Iowa City, IA, USA) and M. Rafieetary (Charles Eye Institute, U.K.) for their kind and helpful assistance in manual grading of tortuosity.

References

[1] D. S. Fong, L. Aiello, T. W. Gardner, G. L. King, G. Blankenship, J. D. Cavallerano, F. L. Ferris, and R. Klein, "Retinopathy in diabetes," *Diabetes Care*, vol. 27, no. suppl. 1, pp. s84–s87, 2004.

[2] H. R. Taylor and J. E. Keeffe, "World blindness: A 21 st century perspective," *Brit. J. Ophthalmol.*, vol. 85, no. 3, pp. 261–266, 2001.

[3] G. Quellec, M. Lamard, P. M. Josselin, G. Cazuguel, B. Cochener, and C. Roux, "Optimal wavelet transform for the detection of microaneurysms in retina photographs," *IEEE Trans. Med. Imag.*, vol. 27, no. 9, pp. 1230–1241, Sep. 2008.

[4] M. Sasongko, T. Wong, T. Nguyen, C. Cheung, J. Shaw, and J. Wang, "Retinal vascular tortuosity in persons with diabetes and diabetic retinopathy," *Diabetologia*, vol. 54, no. 9, pp. 2409–2416, 2011.

[5] M. Mizutani, T. S. Kern, and M. Lorenzi, "Accelerated death of retinal microvascular cells in human and experimental diabetic retinopathy." *J. Clinical Investigation*, vol. 97, no. 12, p. 2883, 1996.

[6] D. K. Wallace, G. E. Quinn, S. F. Freedman, and M. F. Chiang, "Agreement among pediatric ophthalmologists in diagnosing plus and pre-plus disease in retinopathy of prematurity," *J. Amer. Assoc. Pediatric Ophthalmol. Strabismus*, vol. 12, no. 4, pp. 352–356, 2008.

[7] I. C. for the Classification of Retinopathy of Prematurity, "The international classification of retinopathy of prematurity revisited." *Archives Ophthalmol.*, vol. 123, no. 7, p. 991, 2005.

[8] L. A. Wittenberg, N. J. Jonsson, R. P. Chan, and M. F. Chiang, "Computer-based image analysis for plus disease diagnosis in retinopathy of prematurity," *J. Pediatric Ophthalmol. Strabismus*, vol. 49, no. 1, p. 11, 2012.

[9] C. M. Wilson, K. Wong, J. Ng, K. D. Cocker, A. L. Ells, and A. R. Fielder, "Digital image analysis in retinopathy of prematurity: A comparison of vessel selection methods," *J. Amer. Assoc. Pediatric Ophthalmol. Strabismus*, vol. 16, no. 3, pp. 223–228, 2012.

[10] E. Trucco, H. Azegrouz, and B. Dhillon, "Modeling the tortuosity of retinal vessels: Does caliber play a role?" *IEEE Trans. Biomed. Eng.*, vol. 57, no. 9, pp. 2239–2247, Sep. 2010.

[11] W. Lotmar, A. Freiburghaus, and D. Bracher, "Measurement of vessel tortuosity on fundus photographs," *Albrecht von Graefes Archiv Für Klinische und Experimentelle Ophthalmologie*, vol. 211, no. 1, pp. 49–57, 1979.

[12] C. Heneghan, J. Flynn, M. OKeefe, and M. Cahill, "Characterization of changes in blood vessel width and tortuosity in retinopathy of prematurity using image analysis," *Med. Image Anal.*, vol. 6, no. 4, pp. 407–429, 2002.

[13] W. E. Hart, M. Goldbaum, B. Côté, P. Kube, and M. R. Nelson, "Measurement and classification of retinal vascular tortuosity," *Int. J. Med. Informatics*, vol. 53, no. 2, pp. 239–252, 1999.

[14] M. Perez, A. Highes, A. Stanton, S. Thorn, N. Chapman, A. Bharath, and K. Parker, "Retinal vascular tree morphology: A semi-automatic quantification," *IEEE Trans. Biomed. Eng.*, vol. 49, no. 8, pp. 912–917, Aug. 2002.

[15] P. Benitez-Aguirre, M. E. Craig, M. B. Sasongko, A. J. Jenkins, T. Y. Wong, J. J. Wang, N. Cheung, and K. C. Donaghue, "Retinal vascular geometry predicts incident retinopathy in young people with type 1 diabetes a prospective cohort study from adolescence," *Diabetes Care*, vol. 34, no. 7, pp. 1622–1627, 2011.

[16] E. Bullitt, G. Gerig, S. Pizer, W. Lin, and S. Aylward, "Measuring tortuosity of the intracerebral vasculature from MRA images," *IEEE Trans. Med. Imag.*, vol. 22, no. 9, pp. 1163–1171, Sep. 2003.

[17] E. Grisan, M. Foracchia, and A. Ruggeri, "A novel method for the automatic grading of retinal vessel tortuosity," *IEEE Trans. Med. Imag.*, vol. 27, no. 3, pp. 310–319, Mar. 2008.

[18] M. Patasius, V. Marozas, A. Lukosevicius, and D. Jegelevicius, "Evaluation of tortuosity of eye blood vessels using the integral of square of derivative of curvature," in *Proc. EMBEC*, 2005, vol. 5, pp. 20–25.

[19] R. Crosby-Nwaobi, L. Z. Heng, and S. Sivaprasad, "Retinal vascular calibre, geometry and progression of diabetic retinopathy in type 2 diabetes mellitus," *Ophthalmologica*, vol. 228, no. 2, pp. 84–92, 2012.

[20] M. B. Sasongko, T. Y. Wong, T. T. Nguyen, R. Kawasaki, A. J. Jenkins, J. Shaw, C. Robinson, and J. J. Wang, "Serum apolipoproteins are associated with systemic and retinal microvascular function in people with diabetes," *Diabetes*, vol. 61, no. 7, pp. 1785–1792, 2012.

[21] K. Chandrinos, M. Pilu, R. Fisher, and P. Trahanias, "Image processing techniques for the quantification of atherosclerotic changes," UK: University of Edinburgh, DAI Res. Paper, 1998.

[22] K. G. Goh, W. Hsu, M. Li Lee, and H. Wang, "Adris: An automatic diabetic retinal image screening system," *Stud. Fuzziness Soft Comput.*, vol. 60, pp. 181–210, 2001.

[23] A. Kaupp, H. Toonen, S. Wolf, K. Schulte, R. Effert, D. Meyerebrecht, and M. Reim, "Automatic evaluation of retinal vessel width and tortuosity in digital fluorescein angiograms," *Investigative Ophthalmol. Visual Sci.*, vol. 32, no. 4, pp. 863–863, 1991.

[24] F. Ghadiri, H. Pourreza, T. Banaee, and M. Delgir, "Retinal vessel tortuosity evaluation via circular hough transform," in *Proc. 18th Iranian Conf. Biomed. Eng.*, Dec. 2011, pp. 181–184.

[25] F. Ghadiri, S. Zabihi, H. Pourreza, and T. Banaee, "A novel method for vessel detection using contourlet transform," in *Proc. Nat. Conf. Commun.*, Feb. 2012, pp. 1–5.

[26] D. K. Wallace, S. F. Freedman, and Z. Zhao, "Evolution of plus disease in retinopathy of prematurity: Quantification by roptool," *Trans. Amer. Ophthalmological Soc.*, vol. 107, pp. 47–52, 2009.

[27] G. Dougherty and J. Varro, "A quantitative index for the measurement of the tortuosity of blood vessels," *Med. Eng. phys.*, vol. 22, no. 8, pp. 567–574, 2000.

[28] C. Eze, R. Gupta, and D. Newman, "A comparison of quantitative measures of arterial tortuosity using sine wave simulations and 3d wire models," *Phys. Med. Biol.*, vol. 45, no. 9, pp. 2593–2599, 2000.

[29] A. A. Kalitzeos, G. Y. Lip, and R. Heitmar, "Retinal vessel tortuosity measures and their applications," *Exp. Eye Res.*, vol. 106, pp. 40–46, 2013.
[30] M. P. Do Carmo and M. P. Do Carmo, *Differential Geometry of Curves and Surfaces*, vol. 2. Englewood Cliffs, NJ, USA: Prentice-Hall, 1976.
[31] P. J. Flynn and A. K. Jain, "On reliable curvature estimation," in *Proc. IEEE Conf. Comput. Vis. Pattern Recog.*, 1989, vol. 89, pp. 110–116.
[32] D. Coeurjolly, S. Miguet, and L. Tougne, "Discrete curvature based on osculating circle estimation," in *Proc. 4th Int. Workshop Vis. Form*, 2001, pp. 303–312.
[33] J. Bullard, E. Garboczi, W. Carter, and E. Fuller Jr, "Numerical methods for computing interfacial mean curvature," *Comput. Mater. Sci.*, vol. 4, no. 2, pp. 103–116, 1995.
[34] O. I. Frette, G. Virnovsky, and D. Silin, "Estimation of the curvature of an interface from a digital 2d image," *Comput. Mater. Sci.*, vol. 44, no. 3, pp. 867–875, 2009.
[35] R. Pourreza, T. Banaee, H. Pourreza, and R. D. Kakhki, "A radon transform based approach for extraction of blood vessels in conjunctival images," in *Proc. Adv. Artif. Intell.*, 2008, pp. 948–956.
[36] Z. Guo and R. W. Hall, "Parallel thinning with two-subiteration algorithms," *Commun. ACM*, vol. 32, no. 3, pp. 359–373, 1989.
[37] A. Chakravarty and J. Sivaswamy, "A novel approach for quantification of retinal vessel tortuosity using quadratic polynomial decomposition," in *Proc. Indian Conf. Med. Inform.Telemed.*, Mar. 2013, pp. 7–12.
[38] Q. Lau, M. L. Lee, W. Hsu, and T. Y. Wong, "Simultaneously identifying all true vessels from segmented retinal images," *IEEE Trans. Biomed Eng.*, vol. 60, no. 7, pp. 1851–1858, Jul. 2013.
[39] E. Poletti, E. Grisan, and A. Ruggeri, "Image-level tortuosity estimation in wide-field retinal images from infants with retinopathy of prematurity," in *Proc. Annu. Int. Conf. IEEE Eng. Med. Biol. Soc.*, Aug. 2012, pp. 4958–4961.
[40] D. K. Wallace, G. E. Quinn, S. F. Freedman, and M. F. Chiang, "Agreement among pediatric ophthalmologists in diagnosing plus and pre-plus disease in retinopathy of prematurity," *J. Amer. Assoc. Pediatric Ophthalmol. Strabismus*, vol. 12, no. 4, pp. 352–356, 2008.

Masoud Aghamohamadian-Sharbaf was born in 1990. He received the B.Sc. degree in electrical engineering from Ferdowsi University of Mashhad (FUM) in 2012. He is currently working toward the M.Sc. degree in communication systems at the Ferdowsi University of Mashhad (FUM), Mashhad, Iran.

He is also with the Vision Laboratory at FUM and the Eye Image Analysis Research Group. His research interest includes optimization theory, frame theory, information theory, and possible applications of the latter two fields in biomedical engineering.

Hamid Reza Pourreza (SM'12) received the M.Sc. degree in electrical engineering and the Ph.D. degree in computer engineering from Amirkabir University of Technology, Tehran, Iran, in 1993 and 2002, respectively.

He is currently an Associate Professor with the Department of Computer Engineering, Ferdowsi University of Mashhad, Mashhad, Iran. His research interests include image processing and machine vision. He is one of the Founders and an active Member of Eye Image Analysis Research Group.

Touka Banaee received the Graduation degree in general medicine from the Mashhad University of Medical Sciences (MUMS) in 1993 and completed her fellowship in vitreoretina at Medical Center of Shahid Beheshti University of Medical Sciences,Tehran, Iran in 2001.

She is an Ophthalmologist and a Fellow in vitreoretinal diseases and surgeries. She has been a Faculty Member at the School of Medicine, Mashhad University of Medical Sciences (MUMS), Mashhad, Iran, since 2001. As a Consultant in ophthalmology, she has since been actively involved in the undergraduate, residency, and fellowship programs of ophthalmology. She is one of the Founders and an active Member of Eye Research Center and Retina Research Center of MUMS and the Eye Image Analysis Research Group. She has more than 50 national and international papers, and has participated in more than 90 national or international presentations. Her research interests include diabetic retinopathy, image processing in retinal diseases, and vitreoretinal surgeries.